Inorganic Chemistry

Article

pubs.acs.org/IC

Gold Derivatives of Eight Rare-Earth-Metal-Rich Tellurides: Monoclinic $R_7Au_2Te_2$ and Orthorhombic R_6AuTe_2 Types

Ping Chai and John D. Corbett*

Department of Chemistry, Iowa State University, Ames, Iowa 50011, United States

Supporting Information

ABSTRACT: Two series of rare-earth-metal (R) compounds, $R_7Au_2Te_2$ (R = Tb, Dy, Ho) and R_6AuTe_2 (R = Sc, Y, Dy, Ho, Lu), have been synthesized by high-temperature techniques and characterized by X-ray diffraction analyses as monoclinic $Er_7Au_2Te_2$-type and orthorhombic Sc_6PdTe_2-type structures, respectively. Single-crystal diffraction results are reported for $Ho_7Au_2Te_2$, Lu_6AuTe_2, $Sc_6Au_{0.856(2)}Te_2$, and $Sc_6Au_{0.892(3)}Te_2$. The structure of $Ho_7Au_2Te_2$ consists of columns of Au-centered tricapped trigonal prisms (TCTPs) of Ho condensed into 2D zigzag sheets that are interbridged by Te and additional Ho to form the 3D network. The structure of Lu_6AuTe_2 is built of pairs of Au-centered Lu TCTP chains condensed with double Lu octahedra in chains into 2D zigzag sheets that are separated by Te atoms. Tight binding−linear muffin-tin orbital−atomic sphere approximation electronic structure calculations on Lu_6AuTe_2 indicate a metallic property. The principal polar Lu−Au and Lu−Te interactions constitute 75% of the total Hamilton populations, in contrast to the small values for Lu−Lu bonding even though these comprise the majority of the atoms. A comparison of the theoretical results for Lu_6AuTe_2 with those for isotypic Lu_6AgTe_2 and Lu_6CuTe_2 provides clear evidence of the greater relativistic effects in the bonding of Au. The parallels and noteworthy contrasts between $Ho_7Au_2Te_2$ (35 valence electrons) and the isotypic but much electron-richer Nb_7P_4 (55 valence electrons) are analyzed and discussed.

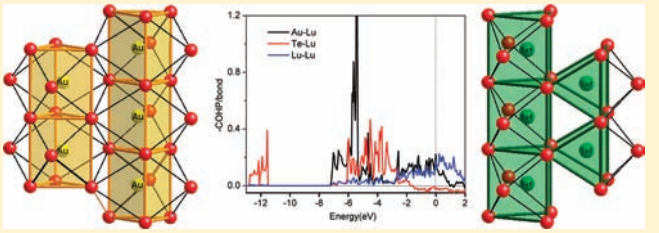

INTRODUCTION

Research into metal-rich compounds has been a consistent highlight in solid-state chemistry because of their diverse structures and, hence, the importance of understanding the relationships among composition, structure, and bonding.[1,2] Among these, metal-rich pnictides, chalcogenides, and halides of the early transition metals have attracted much attention during the past two decades.[3−6] Of special interest are the electron-poorer rare-earth-metal-rich tellurides because they display a wide variety of structural motifs, isolated metal clusters, 1D metal chains, 2D sheets, and 3D networks.

Although many binary rare-earth-metal-rich tellurides have been discovered, the more significant advances occurred when the late transition metals were incorporated into the R-based regions as interstitials. The cluster condensation that follows R-richness and tellurium (Te)-poorness leads to numerous complex structures, such as orthorhombic $Er_7Ni_2Te_2$[7] and $Lu_7Z_2Te_2$ (Z = Ni, Pd, Pt),[8] monoclinic $Er_7Au_2Te_2$,[9] hexagonal R_6ZTe_2 (R = Sc, Dy; Z = Mn, Fe, Co, Ni),[10,11] and orthorhombic Sc_6ZTe_2 (Z = Pd, Ag, Cu, Cd),[12,13] $Sc_5Ni_2Te_2$,[14] $Y_5Z_2Te_2$ (Z = Fe, Co, Ni),[15] and $Lu_5Au_2Te_2$,[16] etc. The strong heterometal interactions between the rare-earth and late transition metals play significant roles in the diversity of their structures, which are, in turn, considerably dependent on the atom sizes, the valence electron concentrations (vec), the proportion of host R to centered Z, and, of course, their relative thermodynamic stabilities.

The incorporation of gold (Au) into different systems, including Zintl phases and icosahedral quasicrystal approximants, has frequently led to new structures with novel bonding,[17−19] in response to Au's unique electronic properties.[20] The participation of Au can simultaneously afford low vec as well as the substantial involvement of $5d^{10}$ states in bonding because of large relativistic effects. Au thereby exhibits a high (Mulliken) electronegativity and thus enhanced polar bond characteristics relative to other metals. These special properties have motivated us to incorporate Au into additional rare-earth-metal-rich telluride systems, inasmuch as only a few examples have been synthesized to date: $Er_7Au_2Te_2$, $Lu_7Au_2Te_2$, $Y_7Au_2Te_2$ and $R_5Au_2Te_2$ (R = Lu, Ho, Dy, Y).[9,16,21] The present paper reports three more Au derivatives of the first type, $R_7Au_2Te_2$ (R = Tb, Dy, Ho), five new Au members for R_6AuTe_2 (R = Sc, Y, Dy, Ho, Lu), and details of their structures and bonding.

EXPERIMENTAL SECTION

Synthesis. All materials were handled in argon-filled gloveboxes with moisture levels below 1 ppm (by volume). The elements were used as received: Sc, Y, Tb, Dy, Ho, and Lu (99.95%, Ames Laboratory), Au (99.995%, Ames Laboratory), and Te pieces (99.99%, Aldrich). To reduce the Te activity in subsequent reactions, all of the syntheses began with the preparation of RTe, for which the elements in a 1:1 molar ratio were sealed inside a silica tube under a high

Received: October 29, 2011
Published: February 24, 2012

   dx.doi.org/10.1021/ic202342v | Inorg. Chem. 2012, 51, 3548−3556

Table 1. Lattice Parameters Refined from Guinier Powder Data for $R_7Au_2Te_2$ (R = Tb, Dy, Ho) and R_6AuTe_2 (R = Sc, Y, Dy, Ho, Lu) Phases

compound	a/Å	b/Å	c/Å	β	volume/Å^3	no. of lines used
$Tb_7Au_2Te_2$	18.215(3)	4.0279(4)	17.164(4)	104.37(1)	1219.8(2)	9
$Dy_7Au_2Te_2$	18.142(4)	4.0134(7)	17.058(2)	104.46(1)	1202.7(2)	9
$Ho_7Au_2Te_2$	17.978(3)	4.0073(6)	16.997(3)	104.427(2)	1185.9(3)	10
$Sc_6Au_{0.89}Te_2$	20.191(4)	3.9199(7)	10.745(1)		850.5(2)	11
Y_6AuTe_2	21.634(5)	4.0931(6)	11.507(1)		1019.0(2)	10
Dy_6AuTe_2	21.610(5)	4.0667(8)	11.438(1)		1005.2(2)	9
Ho_6AuTe_2	21.420(5)	4.0620(8)	11.391(1)		991.1(2)	9
Lu_6AuTe_2	21.0731(5)	4.003(1)	11.267(3)		950.5(3)	9

Table 2. Selected Crystal and Refinement Data for $Ho_7Au_2Te_2$, Lu_6AuTe_2, $Sc_6Au_{0.85}Te_2$, and $Sc_6Au_{0.89}Te_2$

empirical formula	$Ho_7Au_2Te_2$	Lu_6AuTe_2	$Sc_6Au_{0.85}Te_2$	$Sc_6Au_{0.89}Te_2$
cryst syst	monoclinic	orthorhombic	orthorhombic	orthorhombic
space group, Z	$C2/m$ (No. 12), 4	$Pnma$ (No. 62), 4	$Pnma$ (No. 62), 4	$Pnma$ (No. 62), 4
a (Å)	17.978(3)	21.0731(5)	20.110(2)	20.191(4)
b (Å)	4.0073(6)	4.003(1)	3.8869(5)	3.9199(7)
c (Å)	16.997(3)	11.267(3)	10.705(1)	10.745(1)
β (deg)	104.427(2)			
volume (Å^3)	1185.9(3)	950.5(3)	836.8(2)	850.5(2)
d_{calcd} (g/cm^3)	10.102	10.496	5.500	5.473
μ (mm^{-1})	75.495	82.994	26.193	26.459
index ranges	$-23 \le h \le 23$, $-5 \le k \le 5$, $-22 \le l \le 22$	$-26 \le h \le 26$, $-5 \le k \le 5$, $-14 \le l \le 14$	$-26 \le h \le 26$, $-5 \le k \le 5$, $-14 \le l \le 14$	$-26 \le h \le 26$, $-5 \le k \le 5$, $-13 \le l \le 13$
reflns collcd	5204	7913	7053	7055
indep obsd reflns	1299 (R_{int} = 0.0515)	1026 (R_{int} = 0.0706)	996 (R_{int} = 0.0585)	915 (R_{int} = 0.0721)
data/param	1299/69	1026/55	996/56	915/56
GOF on F^2	1.026	1.048	1.125	1.027
R indexes [$I > 2\sigma(I)$]	R1 = 0.0364, wR2 = 0.0716	R1 = 0.0375, wR2 = 0.0794	R1 = 0.0328, wR2 = 0.0640	R1 = 0.0345, wR2 = 0.0649
R indexes (all data)	R1 = 0.0506, wR2 = 0.0771	R1 = 0.0521, wR2 = 0.0844	R1 = 0.0427, wR2 = 0.0681	R1 = 0.0505, wR2 = 0.0709
largest diff peak, hole (e/Å^3)	3.17 [0.94 Å from Ho6], −2.87 [0.98 Å from Ho1]	3.44 [1.06 Å from Lu2], −3.87 [1.16 Å from Te1]	1.66 [0.98 Å from Au], −1.30 [1.43 Å from Sc5]	1.94 [0.98 Å from Au], −2.15 [1.85 Å from Au]

vacuum, slowly heated to 450 °C, held for 12 h, then reacted at 900 °C for 72 h, and finally cooled radiatively. All of the RTe products were single phases when examined by Guinier powder X-ray diffraction (XRD).

The appropriate amounts of RTe, R, and Au on a ∼300 mg scale for R:Au:Te = 7:2:2 stoichiometries were pressed into 10-mm-diameter pellets with the aid of a hydraulic press (Specac) in the glovebox. These were arc-melted for 15 s with ∼20 A current on a copper hearth after zirconium shot had first been melted to further purify the argon atmosphere. The samples were subsequently turned over and arc-melted again to improve the homogeneity. The weight losses during arc melting were under 5%. The buttons were sealed into tantalum tubes and then into evacuated fused silica jackets. These were heated at 1000 °C for 400 h and then allowed to cool radiatively inside the furnace. The isostructural compounds $R_7Au_2Te_2$ (R = Tb, Dy, Ho) with yields above ∼90% plus some RTe impurity phases were obtained according to powder XRD pattern data. Reactions with scandium (Sc) were unproductive, giving only some mixed binary phases.

The R_6AuTe_2 (R = Y, Dy, Ho, Lu) phases were obtained according to the same process, and initial elemental stoichiometries R:Au:Te = 6:1:2. The final annealing step was at 1050 °C for 10 days. All reactions resulted in the target stoichiometric phases in ∼90% yields with small amounts of RTe as impurities according to powder XRD patterns. On the other hand, the product from the parallel reaction with Sc:Au:Te = 6:1:2 gave a refined composition of $Sc_6Au_{0.856(2)}Te_2$ by single-crystal refinement, that is, with ∼14% less Au than expected. Reactions with additional Au were thereby performed. The powder XRD patterns showed that the line positions shifted to lower angles with increased Au, which suggested an increase of the Au content in the phase. A Au content of ∼89(3)% was refined after the loaded proportion was changed to Sc:Au:Te = 6:1.3:2 (below). Further, Au led to no additional line shifts but more impurity phases. The Guinier powder XRD patterns from $Sc_6Au_{0.856(2)}Te_2$ and $Sc_6Au_{0.892(3)}Te_2$ and that calculated from the structure of the latter are provided in Figure S1 in the Supporting Information; the shift with the Au content is clear.

Powder XRD. All of the products were analyzed according to powder XRD patterns recorded in the 2θ range of 4−100° for 30 min with the aid of a Huber Guinier 670 image diffractometer with Cu Kα_1 radiation. Samples were ground to a fine powder and evenly distributed between two Mylar films with the aid of a little petrolatum, which were held between two aluminum rings of the sample holder. Table 1 lists the lattice parameters for all of the compounds as obtained by least-squares refinements of the measured and indexed lines over 2θ = 10−50°.

Single-Crystal Diffraction Studies. Good-quality crystals of $Ho_7Au_2Te_2$, Lu_6AuTe_2, and $Sc_6Au_xTe_2$ were selected for single-crystal XRD data collection on a Bruker AXS SMART APEX CCD-based X-ray diffractometer equipped with monochromatized Mo Kα radiation. Sets of 606 frames with exposure times of 10 s/frame were collected at room temperature for each. The intensities were integrated with *SAINTPLUS*,[22] and absorption corrections were applied with the package program *SADABS*.[23] The *XPREP* subprogram in the *SHELXTL*[24] software package was used for the space group determination and averaging, and the structures were solved by direct methods and refined by a full-matrix least-squares method on F_o^2 with the aid of *SHELXTL-6.10*. The cell and refinement data for four structures are given in Table 1.

$Ho_7Au_2Te_2$. The powder XRD patterns revealed that $Ho_7Au_2Te_2$ is isostructural with the monoclinic $Er_7Au_2Te_2$. Therefore, the space group $C2/m$ was selected directly, and the atom sites were assigned according to the data for $Er_7Au_2Te_2$. The final anisotropic refinement

dx.doi.org/10.1021/ic202342v | Inorg. Chem. 2012, 51, 3548−3556

Table 3. Atomic Coordinates and Isotropic Equivalent Displacement Parameters (Å^2 × 10^4) for $Ho_7Au_2Te_2$ and Lu_6AuTe_2

atom	Wyckoff	symmetry	x	y	z	U_{eq}[a]
			$Ho_7Au_2Te_2$			
Au1	4i	m	0.17125(5)	0	0.11128(6)	152(2)
Au2	4i	m	0.38078(5)	0	0.60065(6)	160(2)
Ho1	4i	m	0.00084(6)	0	0.33326(6)	110(2)
Ho2	4i	m	0.17599(6)	0	0.53257(7)	130(2)
Ho3	4i	m	0.19070(6)	0	0.31877(7)	125(2)
Ho4	4i	m	0.33751(6)	0	0.02033(7)	127(2)
Ho5	4i	m	0.57403(6)	0	0.17184(7)	130(2)
Ho6	4i	m	0.78129(6)	0	0.19476(6)	115(2)
Ho7	2d	2/m	0	0.5	0.5	119(3)
Ho8	2a	2/m	0	0	0	119(3)
Te1	4i	m	0.36639(8)	0	0.33737(9)	101(3)
Te2	4i	m	0.06506(8)	0	0.85018(9)	106(3)
			Lu_6AuTe_2			
Au	4c	m	0.42410(5)	$^1/_4$	0.63237(8)	104(2)
Lu1	4c	m	0.10868(5)	$^1/_4$	0.31371(9)	114(2)
Lu 2	4c	m	0.15787(8)	$^1/_4$	0.02941(9)	76(2)
Lu 3	4c	m	0.26765(5)	$^1/_4$	0.73968(9)	87(2)
Lu 4	4c	m	0.47411(5)	$^1/_4$	0.37815(9)	88(2)
Lu 5	4c	m	0.35986(5)	$^1/_4$	0.06222(9)	84(2)
Lu 6	4c	m	0.00667(5)	$^1/_4$	0.6114(1)	142(3)
Te1	4c	m	0.23678(7)	$^1/_4$	0.4565(1)	74(3)
Te2	4c	m	0.12595(7)	$^1/_4$	0.7681(1)	79(3)

[a] U_{eq} is defined as one-third of the trace of the orthogonalized U_{ij} tensor.

Table 4. Interatomic Distances (Å) and ICOHP Values [eV/bond·mol] in Lu_6AuTe_2[a]

bond	n	distance	ICOHP	bond	n	distance	ICOHP
Au–Lu2	8	2.887(1)	1.17	Lu6–Lu6	4	3.223(1)	0.80
Au–Lu4	8	2.936(1)	1.04	Lu1–Lu6	8	3.260(1)	0.68
Au–Lu1	8	2.942(1)	1.20	Lu1–Lu2	4	3.367(2)	0.34
Au–Lu4	4	3.052(1)	0.95	Lu1–Lu3	8	3.390(1)	0.30
Te1–Lu5	8	3.094(1)	0.83	Lu2–Lu3	8	3.476(1)	0.22
Te1–Lu2	8	3.100(1)	0.76	Lu5–Lu6	8	3.496(1)	0.33
Te1–Lu1	4	3.143(2)	0.72	Lu1–Lu5	8	3.505(1)	0.34
Te1–Lu3	8	3.160(1)	0.76	Lu1–Lu4	4	3.566(2)	0.34
Te1–Lu3	4	3.256(2)	0.47	Lu4–Lu4	4	3.569(1)	0.17
Te2–Lu3	4	3.003(2)	0.93	Lu4–Lu6	8	3.634(2)	0.18
Te2–Lu2	4	3.020(2)	0.96	Lu5–Lu6	4	3.662(2)	0.56
Te2–Lu6	4	3.072(2)	0.81	Lu2–Lu4	8	3.827(1)	0.08
Te2–Lu5	8	3.079(2)	0.76	Te2–Lu4	8	3.161(1)	0.64

[a] n is the number of interactions of each type per cell.

converged at R1 = 3.64% and wR2 = 7.16% for the stoichiometric composition $Ho_7Au_2Te_2$. The difference Fourier map showed featureless residual peaks of +3.17 and −2.87 e/Å^3 that were 0.94 and 0.98 Å from Ho6 and Ho1, respectively.

Lu_6AuTe_2. The powder XRD patterns indicated that Lu_6AuTe_2 is isostructural with the orthorhombic Sc_6PdTe_2, so space group *Pnma* was chosen. A total of 3 out of the 12 sites obtained from direct methods were immediately deleted because of the unreasonable interatomic distances or displacement parameters. The remaining sites were assigned as one Au, two Te, and six Lu according to the differences in the displacement parameters. Convergence was achieved with an R1 value of 5.3%. Further anisotropic refinement converged at R1 = 3.75% and wR2 = 7.94% with the largest Fourier difference map residuals of +3.44 and −3.87 e/Å^3 for 1.06 and 1.16 Å from Lu2 and Te1, respectively.

$Sc_6Au_{0.85}Te_2$ and $Sc_6Au_{0.89}Te_2$. The powder XRD patterns following reactions of normal 6:1:2 loadings indicated the same orthorhombic Sc_6PdTe_2-type structure. Therefore, the same procedures were used, and the anisotropic refinement converged at R1 = 4.82% and wR2 = 12.83%. The large wR2 suggested that something was abnormal, and careful observations indicated unusually large anisotropic displacement parameters (U_{ii}) for Au. Subsequent refinements that allowed the Au occupancy to vary led to a large drop of wR2. The final refinement converged at R1 = 3.28% and wR2 = 6.40% for the composition $Sc_6Au_{0.856(2)}Te_2$, in which the Au site was occupied by 85.6(2)% Au. The only difference Fourier peaks were about ±2 e/Å^3 and near Au atoms. The same refinement procedures were used for a product that had been loaded with 30% excess Au, Sc:Au:Te = 6:1.3:2. The final refinement converged at R1 = 3.45% and wR2 = 6.49% at the composition $Sc_6Au_{0.892(3)}Te_2$, in which the occupancy of the Au site had been increased by 4.2%.

Some crystallographic and refinement data for the four compounds are listed in Table 2. The corresponding atomic coordinates standardized with STRUCTURE TIDY[25] for the first two phases are given in Table 3 together with the isotropic-equivalent displacement parameters. Selected interatomic distances and weighted integration of the crystal orbital Hamilton population (ICOHP) data for Lu_6AuTe_2

dx.doi.org/10.1021/ic202342v | Inorg. Chem. 2012, 51, 3548–3556

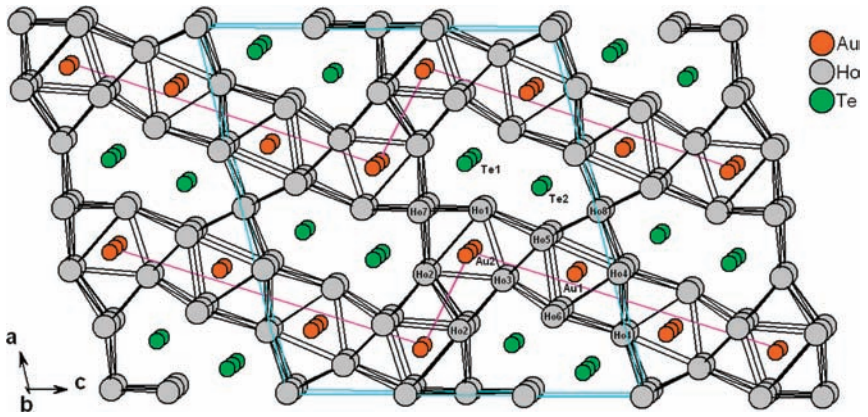

Figure 1. ~[010] view of $Ho_7Au_2Te_2$. Ho, Au, and Te atoms are gray, orange, and green spheres, respectively. The red lines are only to guide the eye along the chain segments.

are shown in Table 4. The remaining Sc results are available in Tables S1 and S2 and in the CIF outputs in the Supporting Information.

Theoretical Calculations. Tight-binding electronic structure calculations were performed for $Ho_7Au_2Te_2$ and Lu_6AuTe_2 according to the linear-muffin-tin-orbital (LMTO) method in the atomic sphere approximation (ASA).[26] The radii of the Wigner–Seitz (WS) spheres were assigned automatically so that the overlapping potentials would be the best possible approximations to the full potentials.[27] For $Ho_7Au_2Te_2$, 19 additional empty spheres (ESs) were introduced per cell ($Z = 4$) within the limit of 18% overlap between an ES and any atom-centered sphere. The WS radii were as follows: Ho, 3.28–3.48 Å; Au, 3.02–3.03 Å; Te, 3.29–3.36 Å; ES, 1.21–2.27 Å. The basis set included Ho 6s/(6p)/5d with Ho $4f^{11}$ treated as the core, Au 6s/6p/5d/(5f), and Te 5s/5p/(5d)/(4f) (downfolded[28,29] orbitals are in parentheses). Exchange and correlation were treated in a local density approximation, and scalar relativistic effects were included. Reciprocal space integrations were performed with the aid of the tetrahedron method.

For Lu_6AuTe_2 ($Z = 4$), 12 additional ESs were introduced within the same limitations. The WS radii were similar: Lu, 3.02–3.42 Å; Au, 3.02 Å; Te, 3.22–3.31 Å; ES, 1.27–2.26 Å. These calculations employed the basis set of Lu 6s/(6p)/5d ($4f^{14}$ as the core), Au 6s/6p/5d/(5f), and Te 5s/5p/(5d)/(4f). Exchange and correlation were again treated in a local density approximation, and scalar relativistic effects were included. For bonding analysis, the energy contributions of filled electronic states for all Lu–Lu, Lu–Au, and Lu–Te contacts were calculated according to the crystal orbital Hamilton population (COHP) method.[30] Weighted integration of COHP data for each bond type over all filled states yielded ICOHP, the Hamilton overlap populations. The tight binding (TB)–LMTO–ASA calculations on Lu_6AgTe_2 and Lu_6CuTe_2 were also carried out for comparison because the previous theoretical consideration for this 6–1–2-type phase was performed at an extended Hückel–TB level and only for Sc_6AgTe_2.[13] The crystal data used were from the original literature,[31] and the calculation procedures were the same as those for Lu_6AuTe_2.

RESULTS AND DISCUSSION

Structural Description of $Ho_7Au_2Te_2$. $Ho_7Au_2Te_2$ crystallizes in a $Er_7Au_2Te_2$-type structure[9] in space group $C2/m$. The ~[010] view of the structure is shown in Figure 1. Au atoms are located in tricapped trigonal prisms (TCTPs) that share trigonal faces to construct infinite 1D columns along b. The TCTPs further interconnect with $b/2$ displacements that lead to alternation of the TP and TC functions and to 2D zigzag sheets along c. Au atoms are distinguished as Au1 and Au2 by their different roles in the zigzag sheets. The Ho2, Ho3, Ho4, and Ho5 members play bifunctional roles: the vertexes of the TP are face-capping atoms on the rectangular face in its neighboring TCTP and vice versa. Finally, the capping atoms Ho7 and Ho8 bridge between the 2D zigzag sheets along [10–1] and [101] to form the 3D network, accompanied by Te1 and Te2 atoms that fill the cavities between the sheets. Figure 2 shows the bonding environments of Te1 and Te2 atoms, which

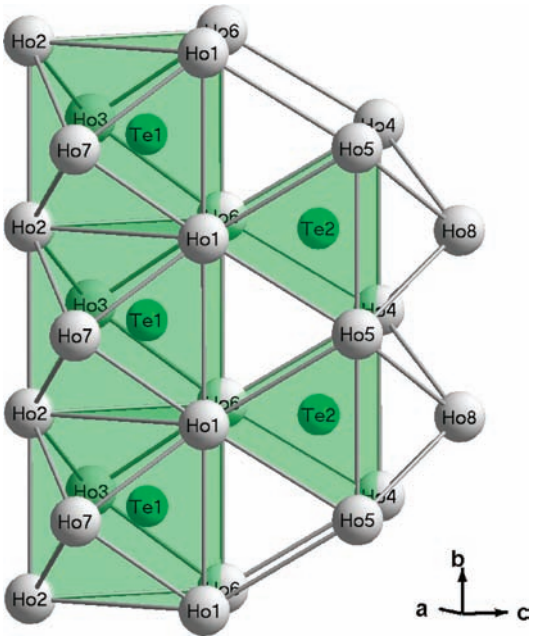

Figure 2. Section of an ~ [100] view of the Te1- and Te2-centered polyhedra in $Ho_7Au_2Te_2$.

center bicapped and monocapped Ho TPs, respectively. The former bicapped prisms parallel the Au-centered TCTP and likewise generate confacial columns along b. The latter monocapped versions lie perpendicular to the former and create 1D chains along b by sharing only Ho4–Ho5 edges. Compared with the member $Er_7Au_2Te_2$,[9] the present $Ho_7Au_2Te_2$ exhibits only general expansions of the distances and the lattice because of the larger size of Ho.

This monoclinic $Ho_7Au_2Te_2$ is a polytype (polymorph) of the older orthorhombic $Er_7Ni_2Te_2$. For comparison, the isotypic $Dy_7Ir_2Te_2$[21] is chosen to represent the latter in the following because iridium (Ir) is closer in size to Au in the present phase. The structure of orthorhombic $Dy_7Ir_2Te_2$ is shown in Figure 3. The 4×2 zigzag Ho_7Au_2 sheets derive from the slightly puckered Dy_7Ir_2 sheets in $Dy_7Ir_2Te_2$. The Ho_7Au_2

dx.doi.org/10.1021/ic202342v | Inorg. Chem. 2012, 51, 3548–3556

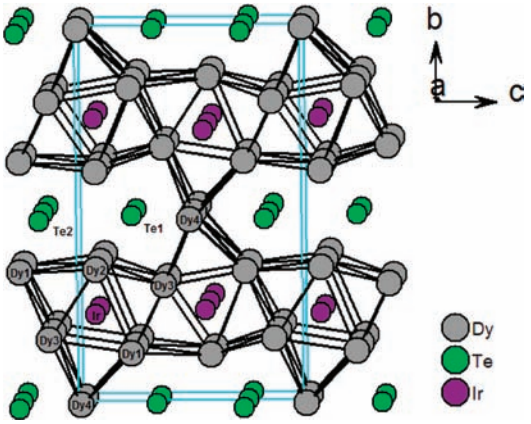

Figure 3. ~[100] view of $Dy_7Ir_2Te_2$. Dy, Ir, and Te atoms are gray, violet, and green, respectively.

sheets are bridged by Ho7 and Ho8 with inversion symmetry, different from those in Dy_7Ir_2, which are connected by bridging Dy4 with mirror symmetry. This packing gives Ho7 and Ho8 one fewer Te neighbor than Dy4 had, but the connection of Ho_7Au_2 sheets becomes more efficient and dense than that of Dy_7Ir_2 sheets. The average Ho7,8–Ho separation is 3.57 Å, in contrast to the corresponding average Dy4–Dy bond of 3.73 Å. Moreover, the Ho7,8–Au distance average is 3.13 Å, which is 0.67 Å less than the Dy4–Ir average. These indicate that a much better packing of Ho_7Au_2 sheets is achieved, given that there is only about a 0.02 Å decrease of the standard metallic radii from Dy to Ho plus a 0.08 Å decrease from Au to Ir.[33] The closer packing of Ho_7Au_2 sheets should be associated with fewer Te neighbors to Ho7 and Ho8 compared with those about Dy4 inasmuch as an increased number of Te neighbors (covalence) is known to detract from the bonding between rare-earth-metal atoms.[32] In other words, the 4 × 2 zigzag Ho_7Au_2 sheets achieve more efficient packing at the expense of one fewer Te neighbor for each of the bridging Ho7 and Ho8. $Ho_7Au_2Te_2$ exhibits a larger difference in the range of d(R–R) than $Dy_7Ir_2Te_2$ does, from 3.474(1) to 4.009(1) Å versus from 3.466(2) to 3.811(2) Å. On the other hand, the ranges of d(R–Z) and d(R–Te) are comparable in the two compounds.

Structural Description of Lu_6AuTe_2. Lu_6AuTe_2 crystallizes in a Sc_6PdTe_2-type structure[12] in space group *Pnma*. Figure 4 shows the ~[010] section of its structure along the short b axis. All atoms lie on mirror planes at $b = {}^1/_4$ or ${}^3/_4$. The Au-centered TCTPs of Lu form infinite 1D chains along b with shared trigonal faces, the same building block as that in $Ho_7Au_2Te_2$. The double TCTP (dTCTP) chains are further condensed with $b/2$ displacements via the shared bifunctional zigzag chains of Lu4 atoms, with inversion points at the centers of the Lu4–Lu4 bonds. The Lu atoms (1–[5,5]–[6,6]–6) form a chain of trans-edge-sharing octahedra along b, which then interconnect via shared Lu6–Lu6 edges to give double octahedral chains with $b/2$ displacements. Inversion centers also lie at the centers of all Lu6–Lu6 edges. The dTCTP and double octahedral chains further interconnect alternately by sharing Lu1–Lu6 edges to generate the 2D zigzag sheets along c, which are separated by Te atoms along a to generate the 3D structure. Te1 and Te2 atoms center bicapped and monocapped TP chains of Lu along b, respectively, the same as those in $Ho_7Au_2Te_2$ (Figure 2).

Lu_6AuTe_2 is isostructural with its ternary neighbors Lu_6AgTe_2 and Lu_6CuTe_2.[31] The standard metallic radii (r_{12})

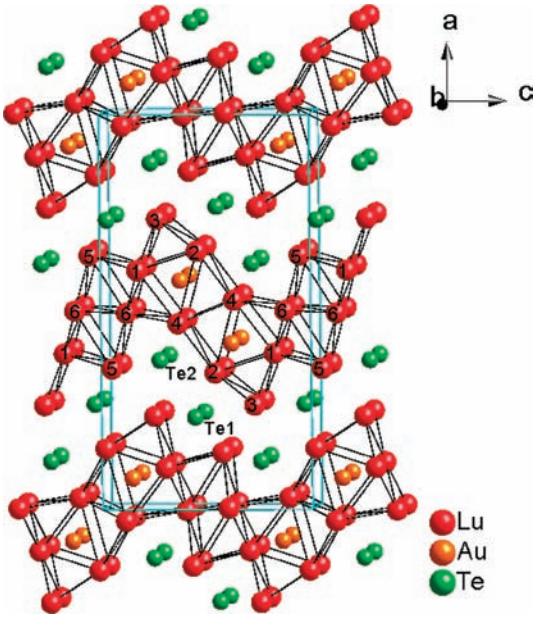

Figure 4. ~[010] view of Lu_6AuTe_2. Lu, Au, and Te atoms are represented by red, orange, and green spheres, respectively.

of these interstitials exhibit an appreciable range, 1.439 Å for Au, 1.442 Å for the slightly larger Ag, and 1.276 Å for Cu,[33] which further indicate the flexible features of this orthorhombic structure. The heteroatomic separations within the TPs naturally also change: 2.89 to 2.94 Å for d(Au–Lu), 2.92 to 2.98 Å for d(Ag–Lu), and 2.86 to 2.92 Å for d(Cu–Lu). (Note the characteristic decrease in the last step.) Simultaneously, the Lu–Lu edges within the TCTP decrease with shrinkage of the interstitial. However, the remaining Lu–Lu bonds within the octahedra and the Lu–Te distances are comparable in all three compounds. These features reveal that the change from Au to Ag and Cu results mainly in the irregular contraction of the TCTP; the average d(Au–Lu), d(Ag–Lu), and d(Cu–Lu) (calculated with inclusion of the distance between the interstitial and capping Lu4) are 2.95, 2.98, and 2.93 Å, respectively. The Au–Lu bond lengths fall between those for Ag–Lu and Cu–Lu rather than much closer to Ag–Lu, as was expected from the slight difference in standard radii between Au and Ag (0.003 Å)[33] and larger differences between Au and Cu (0.163 Å). The shorter Au–Lu bonds should be attributed to the relativistic effects in Au bonding, which is also reflected in the calculation results shown below.

Stoichiometries of $Sc_6Au_{1-x}Te_2$. An unusual result appeared following the first attempt to synthesize the analogous Sc_6AuTe_2; the refined composition was clearly substoichiometric, $Sc_6Au_{0.856(2)}Te_2$, with 14% less Au than expected. This is the first such example among what appears to be a relatively stable series of diverse R–Au–Te phases. Reactions with increased Au proportions showed clear shifts of their powder pattern lines to lower angles. A single crystal from a similar reaction loaded as Sc:Au:Te = 6:1.3:2 refined as $Sc_6Au_{0.892(3)}Te_2$ (Table 1), with a 4.2% increase in the Au content. Powder patterns of these two samples and that calculated from the result of the second refinement are shown in Figure S1 in the Supporting Information, and the customary refinement results, in Tables S1 and S2 in the Supporting Information. Still greater Au contents gave no significant line shifts but increases in byproducts.

dx.doi.org/10.1021/ic202342v | *Inorg. Chem.* 2012, 51, 3548–3556

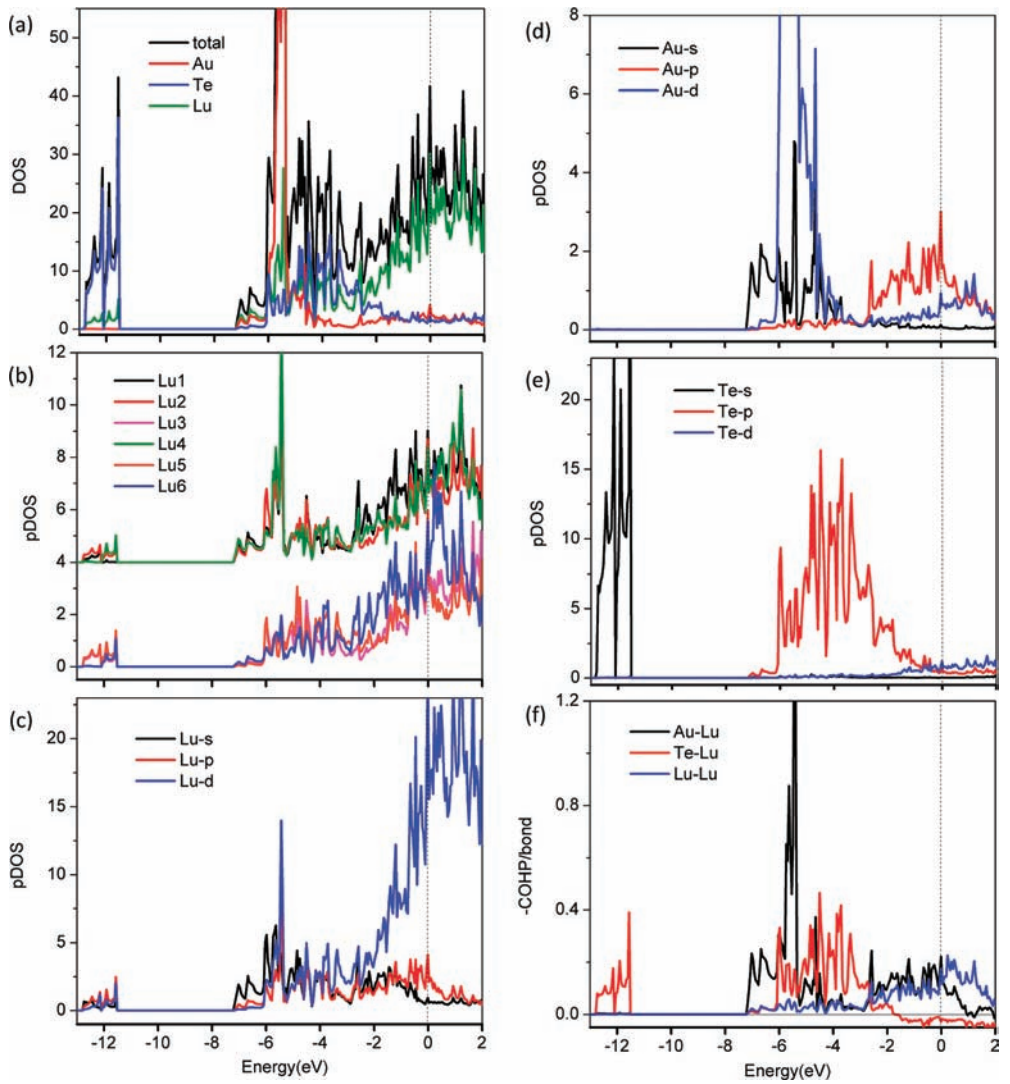

Figure 5. TB–LMTO–ASA electronic structure results for Lu_6AuTe_2. (a) Total DOS and pDOS curves for Lu, Au, and Te. (b) DOS curves for separate Lu atoms. The data for Lu1, Lu2, and Lu4 are raised in order to distinguish them. (c and d) Orbital pDOS data for Lu, Au, and Te. (f) COHP (eV/bond·mol). The dashed lines mark the Fermi energy (E_F). (The comparable data for $Ho_7Au_2Te_2$ appear in Figure S2 in the Supporting Information.)

This thermodynamic effect could be caused by the smaller size of (or lower R–R bond strength for) Sc relative to those of the heavy rare-earth elements ($\Delta r \sim 0.14$ Å) and the resulting strain (bond lengthening) in the host lattice. Note the 1.63% *increase* in the cell volumes and the corresponding *decrease* in the crystal densities that accompany the inclusion of more Au (Table 1), not the opposite that would be expected on filling nominally free space in a lattice. These results clearly support the idea of a size incompatibility between an increased interstitial Au content and the Sc cluster, a matrix effect.

Theoretical Results. The electronic densities of states (DOS) and COHP plots for $Ho_7Au_2Te_2$ are shown in Figure S2 in the Supporting Information. These are very similar to those reported for $Er_7Au_2Te_2$;[9] therefore they will not be discussed further except for comparisons with parallel data for Nb_7P_4 below. The theoretical results for orthorhombic Lu_6AuTe_2 have been analyzed considering that the previous theoretical treatment of the isostructural Sc_6AgTe_2 was performed only at the extended Hückel level.[13] The total DOS, the orbital partial DOS (pDOS) for each atom, and the COHP data for different pairwise interactions are plotted in Figure 5a–f as a function of the energy (eV). Three clearly separated bands are found in the total DOS. The lowest-energy band around −12 eV originates mainly from Te 5s. Among the middle bands within ∼−7 to −2.5 eV, the lower parts are dominated by Au 6s/5d and the higher parts originate about evenly from Te 6p and Lu 6s/6p/5d. A major number of Lu 5d states that continue well above E_F are common evidence for the oxidation of Lu by Au and Te, and these also generate a metallic characteristic for Lu_6AuTe_2.

The orbital pDOS of Lu shows mixed contributions of the 6s, 6p, and 5d states within −13 to −11.5 and −7 eV to E_F, above which the distribution is predominantly from 5d. The former matches distributions of Te 6s and its Lu neighbors. The Lu–Lu COHP results from −2 eV to beyond E_F correlate with the Lu 5d distribution very well, which reflect the main contributions of 5d–5d interactions. The Lu–Au COHP is skewed toward lower region Au 6s/5d states and higher Au 6p. The Au 5d states lie between ∼−7 and −3 eV with a large and quite sharp peak centered at ∼−5.5 eV. Particularly, the Au 6s states fall within the energy range of the Au 5d band, following their obvious relativistic mixing in Au bonding. The Au 6p

dx.doi.org/10.1021/ic202342v | *Inorg. Chem.* 2012, 51, 3548–3556

Table 5. Average ICOHP for Each Bond Type and the Sum per Unit Cell in Lu_6AuTe_2, Lu_6AgTe_2, and Lu_6CuTe_2 (*Pnma*, $Z = 4$)

	Lu_6AuTe_2			Lu_6AgTe_2			Lu_6CuTe_2		
	Lu−Lu	Lu−Au	Lu−Te	Lu−Lu	Lu−Ag	Lu−Te	Lu−Lu	Lu−Cu	Lu−Te
ICOHP (eV/bond· mol)	0.34	1.11	0.76	0.38	0.98	0.85	0.40	0.83	0.82
bonds/cell	76	28	60	76	28	60	76	28	60
ICOHP (eV/cell)	25.8	31.1	45.6	28.9	27.4	51.0	30.4	23.2	49.2
% contribution	25.2	30.3	44.5	26.9	25.6	47.5	29.6	22.5	47.9

states are clearly separated from the 6s,5d states and lie from −2.5 eV to above E_F, reflecting the further reduction of Au. The strong peaks for Lu1, Lu2, and Lu4 at ∼−5.5 eV match the corresponding Lu−Au COHP very well, marking significant bonding between Au and those neighbors. The Lu−Te COHP is skewed toward Te and the lower-lying bands from interactions between Te 6s and Lu 6s, 6p, and 5d, whereas the higher bands arise from interactions of Te 6p with Lu 6s, 6p, and 5d. The Au and Te states are almost filled, matching the substantial oxidation of Lu that is reflected in the distribution of the less penetrating Lu 5d orbitals. Such polar R−Z and R−Te interactions are common in many other related metal-rich compounds.[9,16,34,35]

The energy-weighted integrals of the COHP data (−ICOHP) are better measures of relative bond overlap populations. The distances and molar ICOHP data for all bonds are listed in Table 4, whereas the corresponding average ICOHP for each bond type and the sum for each over the cell are given in Table 5. The average Lu−Au interaction in Lu_6AuTe_2 is the largest, 1.11 eV/bond·mol, relative to Lu−Te, 0.76 eV, and Lu−Lu, 0.34 eV. Obviously, heteroatomic bonding plays significant roles. The numbers of Lu−Au, Lu−Te, and Lu−Lu bonds per cell vary as 28, 60, and 76, giving cumulative ICOHP values of 31.1, 45.6, and 25.8 eV, respectively. The large multiplicity of the Lu−Lu bonds somewhat offsets their much smaller average ICOHP values, but they still comprise the smallest contribution, ∼25% to the total ICOHP. On the other hand, the polar Lu−Au and Lu−Te populations together provide 75% of the total, a common feature in the other metal-rich tellurides. The more frequent Lu−Te bonding makes a 45% contribution to the total, whereas only 30% comes from Lu−Au bonding. The corresponding lower Lu−Au bond proportion in this Au-poorer example makes the Lu−Au bonding distinctively less with respect to the Lu−Te components, in contrast to the R−Au interactions that dominate in many related structures.[2,9,16]

The analogous Lu_6AgTe_2 and Lu_6CuTe_2 provide further evidence for the relativistic effects of Au in Lu_6AuTe_2. Figures S3 and S4 in the Supporting Information contain DOS and COHP data for Lu_6AgTe_2 and Lu_6CuTe_2, and the ICOHP for each bond type and the sum for each phase are listed in Table 5. The three compounds exhibit very similar electronic structure distributions except for the differences in the group 11 member contributions. Similarly, the average Lu−Au, Lu−Ag, and Lu−Cu populations individually remain the largest of the three terms for each, decreasing in that order. In Lu_6CuTe_2, the average Lu−Cu interaction (0.83 eV) is substantially equal to that for Lu−Te (0.82 eV), and the cumulative Lu−Ag and Lu−Cu populations become smaller than those for parallel homoatomic Lu−Lu terms. The large contribution of Lu−Au can be ascribed to the related polar character. The dominance/importance of Au in such parallel population comparisons can in different but interrelated ways be attributed to greater $ns/(n-1)d$ mixing, greater relativistic effects, larger bond populations, a small radius for its position, and an enhanced electronegativity, 5.77 eV, which places it near Te and Se.[36]

$Ho_7Au_2Te_2$ and Nb_7P_4, the Same but Different. A clear isotypism and some interesting chemical differences exist between $Ho_7Au_2Te_2$, $Lu_7Au_2Te_2$,[9] etc., and the long-known Nb_7P_4.[37] A priori attempts to design such ternary or higher polytypes starting from suitably flexible binary (or other) phases that have multiple sites for the same atom types are generally complicated and limited by chemical, thermodynamic, and crystallographic challenges. Rather, accidents and luck (and Pearson's number indexes) usually find them for us. The complex binary metal-rich phosphide Nb_7P_4 was, of course, found accidentally, and the structure, a major accomplishment at that time, was published by Rundquist in 1966.[37] The present and recent $R_7Au_2Te_2$ (R = Tb, Dy, Ho, Er, Lu) examples are the first ternary examples and were again discovered by chance, not planning. The contrasts in the characteristics of the respective atom types are particularly noteworthy.

The metal polyhedra about all four independent anions in the two series are more or less similar, augmented TPs that are not highly constrained by the $C2/m$ symmetry (Figure 1). The relatively undifferentiated polyhedra in the phosphide presumably become split when P1 and P2 atoms are replaced by the larger, electron-poorer, and more strongly bonded Au1 and Au2. Some distortions among bonds to the face-capping R atoms are noticeable, but both are classical TCTP if somewhat longer distances are included in the counts. Conversions of the Nb−P3 and Nb−P4 polyhedra to 0.55 Å longer Ho−Te linkages are less distinctive; in both cases, the coordination about these two are limited to 8- and 7-fold because the next-nearest atoms in this structure are additional Te.

Substantial chemical changes are noteworthy because the 55 valence electrons per formula unit Nb_7P_4 ($7 \times 5 + 5 \times 4$) are converted to the 35-electron $R_7Au_2Te_2$ ($7 \times 3 + 2 \times 1 + 2 \times 6$), a 36% reduction. The change in the cation oxidation states and the Au substitution are the major parts of the difference. Certainly, the introduction of Au atoms for P1 and P2 have the more substantial effects on bonding, Au acting as a sort of early post-transition element with vacant s and p orbitals but with nearby penultimate $5d^{10}$ states that also provide substantial contributions to the bonding, particularly with the open 5d bands (as well as 6s and 6p) on R (Figure 5). The ternary phase yields ICOHP values comparable to those for the phosphide (to the extent that the two sets of results can be compared meaningfully), but the ternary is likely the more polar in terms of Mulliken electronegativities,[36] largely because of Au.

Differences in certain pDOS distributions in the two phase types are most noteworthy (Figure 6). Displacement of substantial fractions of the 5d states on R atoms to above E_F is a familiar signal of its relative oxidation in these and other R−Au−Te compounds, whereas the greater occupation of the Nb 4d valence states on this less oxidized metal is directly related

dx.doi.org/10.1021/ic202342v | Inorg. Chem. 2012, 51, 3548−3556

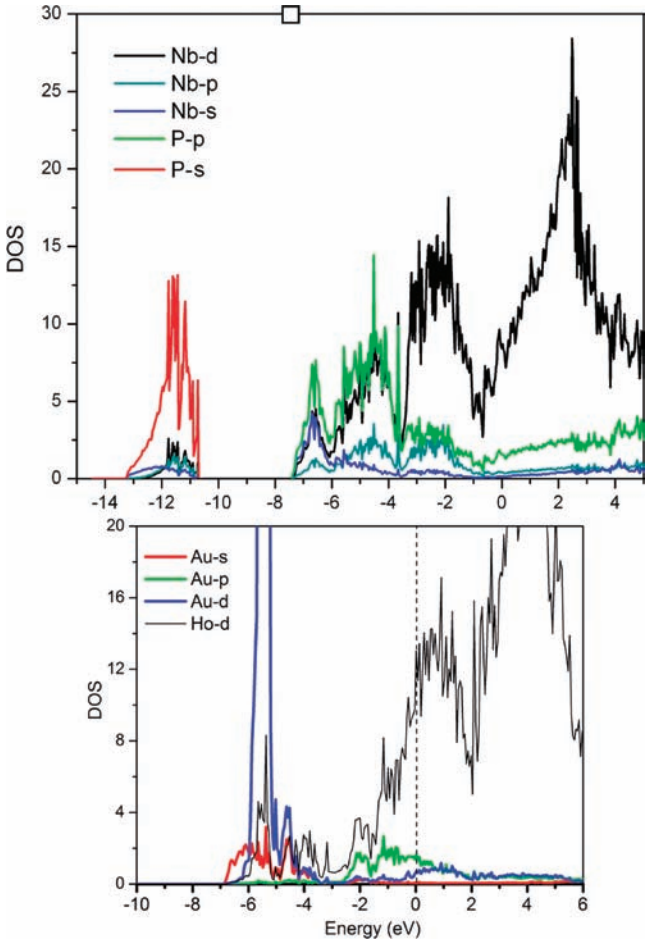

Figure 6. Comparisons of the DOS of the more important Nb 4d and Ho 5d states and of the (d), s, and p orbital states on P versus Au showing how similar these distributions are when compared for the same electron count and scale. The quite similar but higher-lying Nb 4d states reflect its higher valence electron count and E_F, and these are followed by the anion 3p/6p states on P/Au (green). The unmarked Ho 6s/6p distributions follow those of Ho 5d quite well, in parallel with lower-lying Nb 5s and 5p states at the top (blue and blue green). The Au 5d state is the new feature.

its larger electron count and higher E_F. This can be readily seen in the comparative DOS data for the two phases around and below E_F in Figure 6, with the two being aligned according to their relative valence electron counts. (The 35 × 4 electrons per cell at E_F for $Ho_7Au_2Te_2$ in the bottom plot fall at −3.03 eV in the upper Nb_7P_4 portion.) The valence d orbital distributions in both 4d Nb and 5d Ho are quite comparable with this alignment adjustment. Likewise, just below these are the P 3p or Au 6p bonding states plus, lower, Au 6s, and these are admixed with Nb 5p or Ho 6p and 6s. [The Ho 6p and 6s states are not shown for clarity, but they follow, and mix with, Ho 5d below −2 eV in the bottom portion; compare Figure 6b and S2b in the Supporting Information. The more uniform Te 5p contributions lie between −1 and −5 eV, in the "Ho d valley" (Figure 6).] A comparison of the COHP data for the two compounds appears in Figure S5 in the Supporting Information.

Although Zr_7P_4[38] and Hf_7P_4[39] are also known, they represent electronically less striking differences than the comparison of Nb_7P_4 with the R_7Au_2Te family.

CONCLUSIONS

$R_7Au_2Te_2$ (R = Tb, Dy, Ho) and R_6AuTe_2 (R = Sc, Y, Dy, Ho, Lu) are isostructural with $Er_7Au_2Te_2$ and Sc_6PdTe_2, respectively. The first structure consists of zigzag metal layers along *c* that are generated by condensation of Au-centered TCTPs of rare-earth metal into chains that are further interbridged by rare-earth metal and Te atoms to form a 3D network. The second structure type contains heterometallic zigzag sheets in *bc* planes that are separated by isolated Te atoms along *a*. The sheets are made of double Au-centered chains of TCTP R atoms that are interbonded with double chains of R octahedra along *b*. The Lu_6AuTe_2 example again exhibits the particular effects of the substantial reduction of Au and the corresponding oxidation of Lu. The individual Lu−Au interactions make the largest contributions to the bond populations even though Au constitutes only 11 atom % of the compound.

ASSOCIATED CONTENT

Supporting Information

Detailed crystallographic data in CIF format, powder pattern comparisons and tables of crystallographic results for $Sc_6Au_{0.85}Te_2$ and $Sc_6Au_{0.89}Te_2$, anisotropic displacement parameters for $Ho_7Au_2Te_2$ and Lu_6AuTe_2, TB−LMTO−ASA results for $Ho_7Au_2Te_2$, Lu_6AgTe_2, Lu_6CuTe_2, and Nb_7P_4, and a COHP comparison between the first and last phases. This material is available free of charge via the Internet at http://pubs.acs.org.

AUTHOR INFORMATION

Corresponding Author

*E-mail: jcorbett@iastate.edu.

Notes

The authors declare no competing financial interest.

ACKNOWLEDGMENTS

The authors thank Qisheng Lin for the LMTO calculations on Nb_7P_4. This research was supported by the U.S. National Science Foundation, Solid State Chemistry, via Grant DMR-0853732. All of the work was performed in the facilities of Ames Laboratory, U.S. Department of Energy.

REFERENCES

(1) Corbett, J. D. *J. Alloys Compd.* **1995**, *229*, 10.
(2) Corbett, J. D. *Inorg. Chem.* **2010**, *49*, 13.
(3) Hughbanks, T. R. *J. Alloys Compd.* **1995**, *229*, 40.
(4) Kleinke, H. *Chem. Soc. Rev.* **2000**, *29*, 411.
(5) Corbett, J. D. *Inorg. Chem.* **2000**, *39*, 5178.
(6) Corbett, J. D. In *Inorganic Chemistry*; Focus, I. I., Meyer, G., Naumann, D., Wesemann, L., Eds.; Wiley-VCH: New York, 2005; Vol. 2, Chapter 8.
(7) Meng, F. Q.; Hughbanks, T. *Inorg. Chem.* **2001**, *40*, 2482.
(8) Chen, L.; Corbett, J. D. *Inorg. Chem.* **2004**, *43*, 3371.
(9) Gupta, S.; Corbett, J. D. *Dalton Trans.* **2010**, *39*, 6074.
(10) Maggard, P. A.; Corbett, J. D. *Inorg. Chem.* **2000**, *39*, 4143.
(11) Bestaoui, N.; Herle, P. S.; Corbett, J. D. *J. Solid State Chem.* **2000**, *155*, 9.
(12) Maggard, P. A.; Corbett, J. D. *J. Am. Chem. Soc.* **2000**, *122*, 10740.
(13) Chen, L.; Corbett, J. D. *Inorg. Chem.* **2002**, *41*, 2146.
(14) Maggard, P. A.; Corbett, J. D. *Inorg. Chem.* **1999**, *38*, 1945.
(15) Maggard, P. A.; Corbett, J. D. *Inorg. Chem.* **2004**, *43*, 2556.
(16) Chai, P.; Corbett, J. D. *Inorg. Chem.* **2011**, *50*, 10949.
(17) Li, B.; Corbett, J. D. *Inorg. Chem.* **2007**, *46*, 6022.
(18) Li, B.; Corbett, J. D. *Inorg. Chem.* **2008**, *47*, 3610.

(19) Lin, Q.; Corbett, J. D. *J. Am. Chem. Soc.* **2007**, *129*, 6789.
(20) Pyykkö, P. *Chem. Rev.* **1988**, *88*, 63.
(21) Herzmann, N.; Gupta, S.; Corbett, J. D. *Z. Anorg. Allg. Chem.* **2009**, *635*, 848.
(22) *SMART*; Bruker AXS, Inc.: Madison, WI, 1996.
(23) Blessing, R. H. *Acta Crystallogr.* **1995**, *A51*, 33.
(24) *SHELXTL*; Bruker AXS, Inc.: Madison, WI, 2000.
(25) Gelato, L. M.; Parthé, E. *J. Appl. Crystallogr.* **1987**, *20*, 139.
(26) Tank, R.; Jepsen, O.; Burkhardt, A.; Andersen, O. K. *TB–LMTO–ASA Program*, version 4.7; Max-Planck-Institut für Festörperforschung: Stuttgart, Germany. 1994.
(27) Jepsen, O.; Andersen, O. K. *Z. Phys. B* **1995**, *97*, 35.
(28) Lambrecht, W. R. L.; Andersen, O. K. *Phys. Rev. B* **1986**, *34*, 2439.
(29) Lowdin, P. J. *J. Chem. Phys.* **1951**, *19*, 1396.
(30) Dronskowski, R.; Blochl, P. E. *J. Phys. Chem.* **1993**, *97*, 8617.
(31) Castro-Castro, L. M.; Chen, L.; Corbett, J. D. *J. Solid State Chem.* **2007**, *180*, 3172.
(32) Pauling, L. *The Nature of the Chemical Bond*, 3rd ed.; Cornell University Press: Ithaca, NY, 1960; p 403.
(33) Maggard, P. A.; Corbett, J. D. *J. Am. Chem. Soc.* **2000**, *122*, 838.
(34) Gupta, S.; Meyer, G.; Corbett, J. D. *Inorg. Chem.* **2010**, *49*, 9949.
(35) Chai, P.; Corbett, J. D. *Inorg. Chem.* **2011**, *50*, 10949.
(36) Pearson, R. G. *Inorg. Chem.* **1988**, *27*, 734.
(37) Rundquist, S. *Acta Chem. Scand.* **1966**, *20*, 2427.
(38) Altzen, P.-J.; Rundquist, S. *Z. Kristallogr.* **1989**, *189*, 149.
(39) Kleinke, H.; Franzen, H. F. *Angew. Chem., Int. Ed. Engl.* **1996**, *35*, 1934.